(14) A. Barkott and C. A. Angell, *J. Phys. Chem.*, **79**, 2192 (1975).
(15) B. D. Bird and P. Day, *J. Chem. Phys.*, **49**, 392 (1968).
(16) (a) O. Kubaschewski, E. Evans, and C. B. Alcock, "Metallurgical Thermochemistry", Pergamon, 1967; (b) *Natl. Bur. Stand. (U.S.), Tech. Note*, **No. 270 (1-7)** (1965-1973); (c) C. E. Wicks and F. E. Black, *U.S., Bur. Mines, Bull.*, **No. 605** (1973).
(17) The calculations were based on thermodynamic data reported in the following references: (a) Al_2Cl_6–$CoCl_2$, ref 3; (b) Al_2Br_6–$CoBr_2$, this work; (c) Ga_2Cl_6–$CoCl_2$, ref 5; (d) Fe_2Cl_6–$CoCl_2$, E. W. Dewing, *Metall. Trans.*, **1**, 2169 (1970).

Contribution from the Department of Chemistry, University of Wyoming, Laramie, Wyoming 82071

Physical Properties of Linear-Chain Systems. 7. Magnon Sidebands in the Electronic Absorption Spectra of $CsCoCl_3$ and $RbCoCl_3$[1]

CHARLES F. PUTNIK and SMITH L. HOLT*[2]

Received November 1, 1976 AIC607783

The polarized, single-crystal absorption spectra of the linear-chain materials $CsCoCl_3$ and $RbCoCl_3$ have been measured at several temperatures between 298 and 4.2 K. Spectral analysis reveals a surprising number of magnon sidebands which have been carefully examined. The sidebands are found to persist to temperatures well above the three-dimensional, antiferromagnetic ordering temperature of the materials. The thermal behavior of the sidebands exhibits a strong correlation with the results obtained from magnetic susceptibility and neutron diffraction measurements. The results indicate that long-range spin correlation exists in one dimension over a wide span of temperature above the Neël point. It appears that this region of one-dimensional spin correlation is a quasi-intermediate phase between three-dimensional magnetic order and paramagnetism in these compounds. The results also expose new facets relating to the mechanism of sideband absorption with which theory may be refined.

Introduction

There are now a number of examples of intensity enhancement of formally spin-forbidden ($\Delta S \neq 0$) electronic transitions in magnetically concentrated systems.[3] Mechanisms have been postulated for the relaxation of the $\Delta S = 0$ spin selection rule and theoretical predictions of the temperature dependence of the exchange-enhanced oscillator strengths have been offered.[4-17] In an effort to ascertain whether the proposed mechanisms are applicable to systems in which the exchange interactions are predominantly one-dimensional, we have investigated a series of compounds of the formulation ABX_3. This class of compounds includes materials where B is any divalent, first-row transition metal ion; A is Rb^+, Cs^+, or any of several alkylammonium cations; and X is either Cl^-, Br^-, or I^-.[18] All compounds of interest crystallize in a hexagonal cell with linear chains of face-sharing $[BX_6]^{4-}$ octahedra extending along the c crystallographic axis. The A cations occupy sites between adjacent chains and the resulting separation provides an effective interchain "magnetic insulation".

Our optical investigations of materials of this type have centered upon the compounds $ANiX_3$ [$A^+ = (CH_3)_4N^+$, Rb^+, Cs^+; $X^- = Cl^-$, Br^-],[19] $AFeX_3$ [$A^+ = Cs^+$, Rb^+; $X^- = Cl^-$, Br^-],[3] $CsMnBr_3$,[20] $RbMnBr_3$,[21] $(CH_3)_4NMnBr_3$,[22] and $ACrCl_3$ [$A^+ = Rb^+$, Cs^+].[1] In all cases we have found evidence of cooperative electronic transitions in which formal spin-selection rules are relaxed but have observed that the temperature dependence of oscillator strengths of individual "spin-forbidden" transitions within a compound and between compounds can vary markedly.

In the present work we have extended our measurements to $CsCoCl_3$ and $RbCoCl_3$. We have recorded the behavior of exchange-assisted "spin-forbidden" transitions and have identified exciton minus magnon sidebands (magnon hot bands), exciton plus magnon sidebands (magnon cold bands), and the associated excitonic origin peaks in these one-dimensional magnetic systems.

Crystal Structures. Soling has reported the crystal structures of $CsCoCl_3$[23] and $RbCoCl_3$.[24] Both crystallize in the space group $P6_3/mmc$ with two formula units per primative cell. The cell dimensions are $a = 7.2019$ (4) Å and $c = 6.0315$ (5) Å for $CsCoCl_3$ and $a = 6.999$ (1) Å and $c = 5.996$ (1) Å for $RbCoCl_3$. These compounds are isostructural with $CsNiCl_3$, the predominant structural feature being linear chains of face-sharing $[CoCl_6]^{4-}$ octahedra lying along the c axis.

Magnetic Properties. The transition to antiferromagnetic order in $CsCoCl_3$ has been determined to occur at 21.5 K from neutron diffraction measurements.[25] The Neël temperature of $RbCoCl_3$ has not been reported but in comparison to other members of this class of compounds it is expected to be some 5–10 K above that of $CsCoCl_3$ (e.g., for $RbCoBr_3$, $T_N = 36$ K;[26] for $CsCoBr_3$, $T_N = 28$ K;[27] for $RbNiCl_3$, $T_N = 11$ K;[28] and for $CsNiCl_3$, $T_N = 4.5$ K[28]).

At 4.2 K the magnetic structure of $CsCoCl_3$ consists of antiferromagnetic planes stacked antiferromagnetically along the c axis.[25] Between 8 K and T_N a different magnetic structure exists which has not been characterized. A similar change occurs in the isostructural material $CsCoBr_3$.[27] In that compound the spin structure at low temperature is essentially the same as for $CsCoCl_3$ but with a slight canting of the spins off the c axis. In the structure which exists between 14 K and T_N one-third of the chains are disordered and the other two-thirds are antiferromagnetically coupled in the basal plane.

Experimental Section

Deep blue single crystals of $CsCoCl_3$ and $RbCoCl_3$ were prepared as described previously with anhydrous $CoCl_2$ and the appropriate alkali chloride was used as starting material.[20] Preparation of thin crystals (0.020–0.025 cm) suitable for σ and π spectral measurements was facilitated by the easy cleavage of the crystals in planes parallel to the c crystallographic axis. The high resistance of the crystals to cleavage perpendicular to the c axis prevented our obtaining samples suitable for axial measurements. Our spectrometer and cryogenic system have been described earlier.[20]

Results

The general features of the spectra of $CsCoCl_3$ and $RbCoCl_3$ are very similar and will be presented simultaneously. The spectra will be described under the general headings of the transitions between the octahedral crystal field states of the d^7 electronic configuration. More detailed analysis including

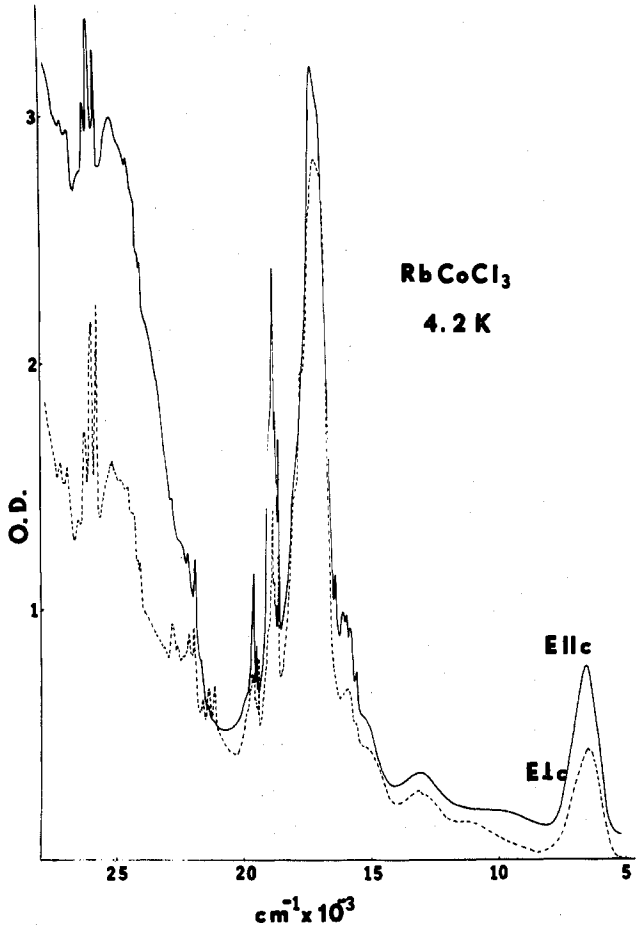

Figure 1. Polarized, single-crystal absorption spectrum of $RbCoCl_3$ at 4.2 K. Optical density is in arbitrary units.

the actual D_{3d} metal ion site symmetry and spin–orbit coupling was not attempted since the theoretical basis for such analysis is incomplete. The magnon sidebands are presented separately since the observations of these anomalous absorptions are the major result of this work. To deal systematically with the large number of observed sidebands they are presented in order of increasing energy under the headings of the d^7 octahedral crystal field states with which they are associated.

Crystal Field Spectra. The polarized, single-crystal absorption spectra of $RbCoCl_3$ and $CsCoCl_3$ at 4.2 K are presented in Figures 1 and 2, respectively. The complex regions between 18 500 and 20 500 cm^{-1} in the spectra of both materials are expanded in Figures 3 and 4 and are also shown at 80 K in these figures.

$^4T_1(F) \rightarrow {}^4T_2(F)$. This spin-allowed absorption is observed at 6300 cm^{-1} in $CsCoCl_3$ and at 6400 cm^{-1} in $RbCoCl_3$. There is no difference in the location of the absorption maxima between polarizations in either compound. The $E \parallel c$ absorption appears as an intense, broad, symmetric band in both cases while the less intense $E \perp c$ component shows slight asymmetry in each. Between room temperature and 80 K the oscillator strength of this transition decreases by 30% and then remains constant as temperature is lowered to 4.2 K. The oscillator strength is on the order of 10^{-5}, as expected for an octahedral spin-allowed transition.

$^4T_1(F) \rightarrow {}^2E(G)$. This absorption is observed near 10 500 cm^{-1} in both systems. It appears as a very broad, weak band which shows little dependence on polarization or temperature.

$^4T_1(F) \rightarrow {}^4A_2(F)$. This absorption is centered near 13 000 cm^{-1} in the $ACoCl_3$ materials and appears as a broad, weak band. While this transition is spin allowed, it is less intense than some of the spin-forbidden transitions. The lack of

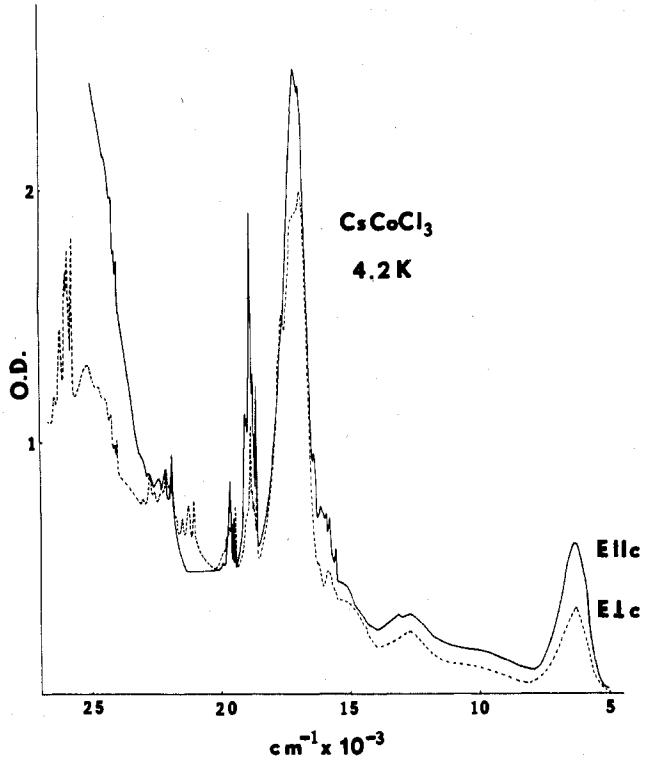

Figure 2. Polarized, single-crystal absorption spectrum of $CsCoCl_3$ at 4.2 K. Optical density is in arbitrary units.

intensity can be understood qualitatively if the strong-field approximation is employed. The ground state derives from the $t_2^5e^2$ configuration and the $^4A_2$ excited state from the $t_2^3e^4$ configuration. It can be seen that a transition from the ground state to the $^4A_2$ excited state is a two-electron process and will have a decreased transition probability in relation to a one-electron transition.

$^4T_1(F) \rightarrow {}^2T_1, {}^2T_2(G)$. The absorptions corresponding to these transitions will be described together since the octahedral levels are close in energy and spin–orbit coupling causes significant overlap. These absorptions appear as a complex manifold centered near 15 800 cm^{-1} in both systems. The $E \parallel c$ components exhibit considerably sharper fine structure than the $E \perp c$ counterparts below 100 K. The strong overlap of this manifold with the $^4T_1(P)$ absorption precludes determination of oscillator strength. Magnon sidebands are observed at the low-energy edge of this manifold in $CsCoCl_3$ with $E \parallel c$.

$^4T_1(F) \rightarrow {}^4T_1(P)$. This very intense manifold is centered near 17 000 cm^{-1} in $CsCoCl_3$ and near 17 200 cm^{-1} in $RbCoCl_3$. This band is the most intense feature in each spectrum and in both cases the $E \parallel c$ components are somewhat more intense than those observed with $E \perp c$. The oscillator strengths of these bands are on the order of 10^{-4}–10^{-5}. Accurate determination of the oscillator strength was not possible due to overlap with adjacent absorptions on both the high- and low-energy sides. Qualitatively, the oscillator strength of this transition decreases by ~30% as temperature is lowered from room temperature to 80 K and remains essentially constant as temperature is further reduced to 4.2 K. Some structure is apparent at 4.2 K but is poorly resolved.

$^4T_1(F) \rightarrow {}^2T_1(P)$. This anomalously intense absorption ($f \approx 10^{-6}$) appears as a complex manifold near 18 800 cm^{-1} in each compound. The $E \parallel c$ components are more intense in each case and both orientations exhibit a number of sharp peaks and shoulders (Figures 3 and 4). Magnon sidebands are observed at the low-energy edge of this manifold in both polarizations. These will be described more fully in the

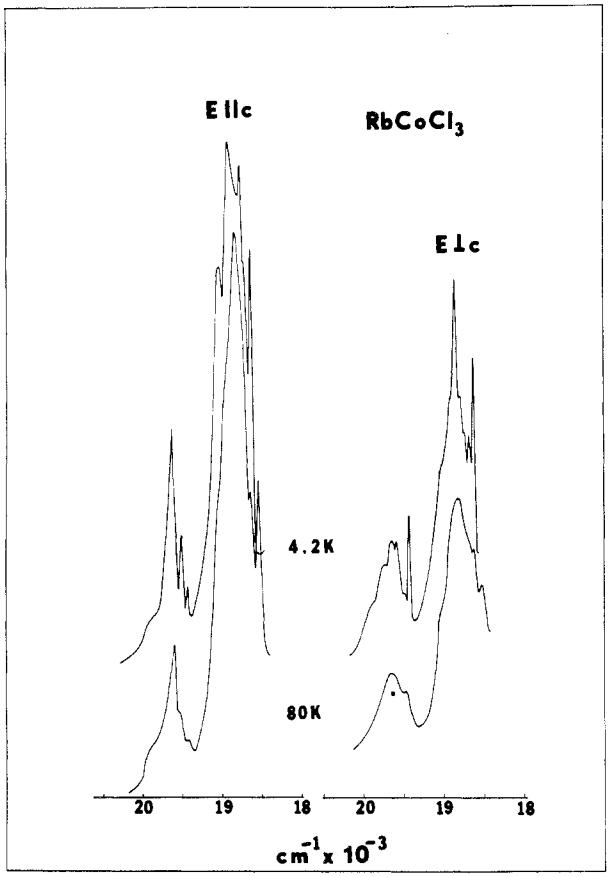

Figure 3. Regions of the $^2T_1(P)$ and $^2A_1(G)$ octahedral, crystal field absorptions in $RbCoCl_3$ from the polarized, single-crystal spectra at 4.2 and 80 K. Note the sidebands on the low-energy absorption edge of each band.

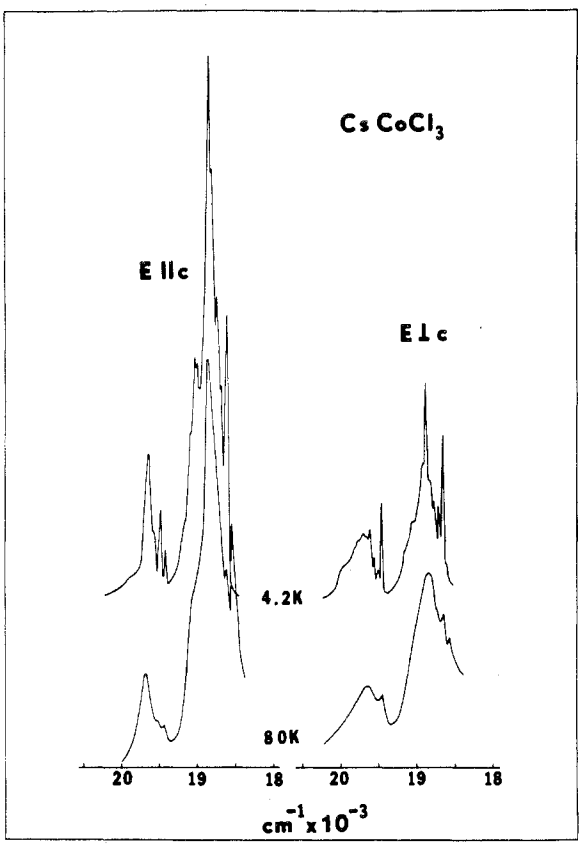

Figure 4. Regions of the $^2T_1(P)$ and $^2A_1(G)$ octahedral, crystal field absorptions in $CsCoCl_3$ from the polarized, single-crystal spectra at 4.2 and 80 K. Note the sidebands on the low-energy absorption edge of each band.

following section and can be identified comparing the 4.2- and 80-K measurements shown in Figures 3 and 4.

$^4T_1(F) \rightarrow {}^2A_4(G)$. This absorption consists of a series of sharp absorptions centered near 19 600 cm^{-1} in both compounds. The total oscillator strength ($\sim 10^{-6}$) shows no large dependence on polarization although several components are polarized in the opposite sense (Figures 3 and 4). Magnon sidebands are observed at the low-energy edge of this absorption in both materials.

$^4T_1(F) \rightarrow {}^2T_2(H)$. This manifold is observed only with $E \perp c$ and consists of four components of vibronic origin in both $CsCoCl_3$ and $RbCoCl_3$. In $CsCoCl_3$ the maxima observed at 21 075, 21 298, 21 527, and 21 763 cm^{-1} appear to be components of an $\sim$225-cm^{-1} progression built upon the 21 075-cm^{-1} origin peak. The three low-energy components of this progression are well-resolved peaks and the highest energy component is a shoulder on the low-energy edge of the adjacent $^2T_1(H)$ manifold. Intensity variation with temperature indicates the 21 075-cm^{-1} peak is of magnon cold-band nature as it steadily decreases in intensity as temperature is raised. A strongly overlapped band some 35 cm^{-1} to lower energy appears at 20 K and steadily gains intensity as the temperature is raised to 60 K.

The appearance and temperature dependence of the analogous absorption in $RbCoCl_3$ are very nearly identical. In this case the progression is based on a 21 178-cm^{-1} origin with $\sim$225-cm^{-1} components observed at 21 401, 21 631, and 21 850 cm^{-1}.

These absorptions represent the only observed phonon progressions which can be assigned with certainty. Evidence is present for progressions in other manifolds; however, the overlap of progressions and the uncertain effect of the trigonal field on the spin–orbit levels limits such assignments to possibly misleading speculation.

$^4T_1(F) \rightarrow {}^2T_1(H)$. This absorption appears as a structured manifold centered near 22 250 cm^{-1} in both orientations of $CsCoCl_3$ and with $E \perp c$ in $RbCoCl_3$. It appears as a series of shoulders on the charge-transfer edge with $E \parallel c$ in $RbCoCl_3$.

$^4T_1(F) \rightarrow {}^2E(H)$. This absorption appears as a broad, asymmetric manifold exhibiting ill-resolved structure. It is centered near 25 000 cm^{-1} and is resolved with $E \perp c$ in both systems, appears high on the charge-transfer edge of $RbCoCl_3$ with $E \parallel c$, and is obscured by the charge-transfer edge in $CsCoCl_3$ with $E \parallel c$. The oscillator strength is in the range of 10^{-6} and shows little dependence on polarization in $RbCoCl_3$.

$^4T_1(F) \rightarrow {}^2T_2(D)$. The final d–d absorption manifold observed in these systems is centered near 26 000 cm^{-1}. It is obscured by the charge-transfer edge in $CsCoCl_3$ with $E \parallel c$ and appears high on the charge-transfer edge of $RbCoCl_3$ in the same orientation. With $E \perp c$ the manifold is well resolved in both materials and appears as a progression of sharp peaks which successively decrease in intensity toward higher energy. The shape and appearance of the bands suggest a phonon nature for the progression but the spacing is inconsistent. Additionally, there is a well-resolved doubling in the second peak which may be a second origin or a component of an overlapped progression. As with the $^2T_2(H)$ absorptions, the low-energy component appears to be of magnon cold-band nature and will be described in the following section.

Magnon Sidebands. Magnon sidebands are observed at the low-energy absorption edge of the $^2T_1$–$^2T_2(G)$, $^2T_1(P)$, $^2A_1(G)$, $^2T_2(H)$, $^2E(H)$, and $^2T_2(D)$ absorption bands in $CsCoCl_3$ and the $^2T_1(P)$, $^2A_1(G)$, $^2T_2(H)$, and $^2T_2(D)$ absorption bands in $RbCoCl_3$. Measurements were made in 5-K increments

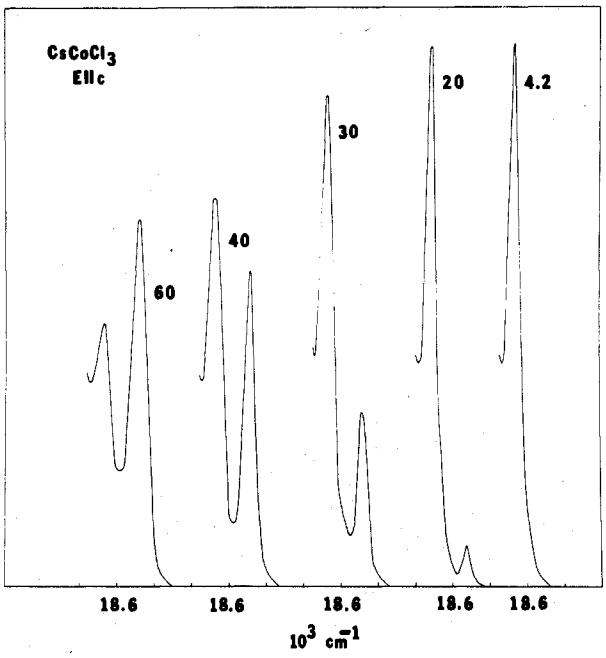

Figure 5. Sidebands associated with the $^2T_1(P)$ absorption in $CsCoCl_3$ with $E \parallel c$ at several temperatures.

between 4.2 and 80 K on several crystals of each compound to ensure accuracy of results. Measurements were also made at 100 and 120 K above which resolution of sharp features was minimal. The sidebands presented in the following figures are those which are well resolved and representative of shape and behavior.[3] The temperature dependence of the sidebands is presented as plots of $f(T)/f_{max}$ vs. temperature. This method normalizes the maximum oscillator strengths of all sidebands and facilitates comparison of thermal behavior.

$^4T_1 \rightarrow {}^2T_1$–$^2T_2$(G). At the low-energy edge of this absorption near 15 500 cm^{-1} in $CsCoCl_3$ with $E \parallel c$ a hot-band, cold-band pair is observed. The cold band, located at 15 547 cm^{-1} at 4.2 K, persists up to 60 K. The hot band first appears at 20 K at 15 456 cm^{-1} and is resolved up to 80 K.

$^4T_1 \rightarrow {}^2T_1$(P). In $CsCoCl_3$ and $RbCsCl_3$ with $E \parallel c$ and with $E \perp c$ hot-band, cold-band combinations are observed near 18 600 cm^{-1}. For both systems with $E \perp c$ the exciton line is also resolved. The $E \parallel c$ absorptions in $CsCoCl_3$ are presented in Figure 5, and the temperature dependences of the components, in Figure 6. The cold band is resolved between 4.2 and 60 K while the hot band appears at 15 K and is resolved up to 80 K. The $E \perp c$ hot-band, cold-band/exciton absorption in $CsCoCl_3$ is presented in Figure 7, and the temperature dependence is presented with that of the parallel component in Figure 6. The cold band is observed at 18 617 cm^{-1}, the exciton at 18 569 cm^{-1}, and the hot band at 18 519 cm^{-1} above 15 K. Resolution of all levels is lost about 80 K.

A cold band is observed at 18 629 cm^{-1} and persists above 80 K while a hot band appears above 15 K at 18 519 cm^{-1} and is still resolved above 120 K. For the $E \perp c$ sidebands of $RbCoCl_3$ a cold band at 18 613 cm^{-1} and an exciton at 18 553 cm^{-1} are observed from 4.2 through 80 K. A hot band at 18 510 cm^{-1} appears above 25 K and is resolved through 120 K.

$^4T_1 \rightarrow {}^2A_1$(G). In $CsCoCl_3$ with $E \perp c$ a cold-band, hot-band pair is observed at 19 450 cm^{-1} and 19 418 cm^{-1}, respectively. The cold band persists through 65 K and the hot band appears at 30 K and persists to 80 K. The overlap of these bands precludes accurate determination of the variation of oscillator strength with temperature. In $RbCoCl_3$ with $E \perp c$ a cold band is observed at 19 425 cm^{-1} which persists through 100 K. This is the only isolated sideband observed. With $E \parallel c$ the spectrum of $RbCoCl_3$ exhibits a hot-band and two-cold band absorptions at 19 420, 19 455, and 19 513 cm^{-1}, respectively. The cold bands are resolved through 100 K and the hot band is resolved from 35 through 120 K.

$^4T_1 \rightarrow {}^4T_2$(H). With $E \perp c$ both systems exhibit cold-band, hot-band pairs near 21 100 cm^{-1}. In both cases the strong overlap prevents accurate measurement of band shape or temperature dependence. In $RbCoCl_3$ the cold band occurs at 21 162 cm^{-1} and persists through 100 K. The hot band appears above 30 K at 21 060 cm^{-1} and also persists through 100 K. In $CsCoCl_3$ the cold band occurs at 21 075 cm^{-1} and the hot band at 21 002 cm^{-1} above 25 K. Both are resolved up to 80 K.

$^4T_1 \rightarrow {}^2E$(H). In $CsCoCl_3$ with $E \perp c$ a cold-band, hot-band pair is observed at 24 015 and 23 915 cm^{-1}, respectively. The hot band appears above 15 K and both are resolved through 80 K. The appearance of these bands is similar to that presented in Figure 5.

$^4T_1 \rightarrow {}^2T_2$(D). With $E \perp c$ in both materials a cold-band, hot-band pair is observed at the low-energy edge of this d–d manifold. Only in $CsCoCl_3$ was good resolution obtained and this is presented in Figure 8. The measured temperature

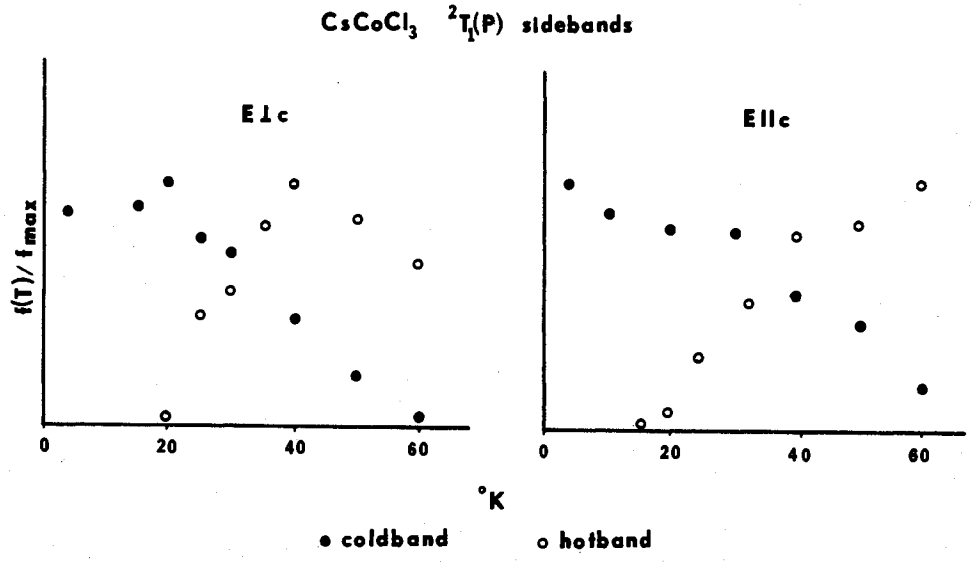

Figure 6. Temperature dependence of the oscillator strengths of the sidebands associated with the $^2T_1(P)$ absorption in $CsCoCl_3$.

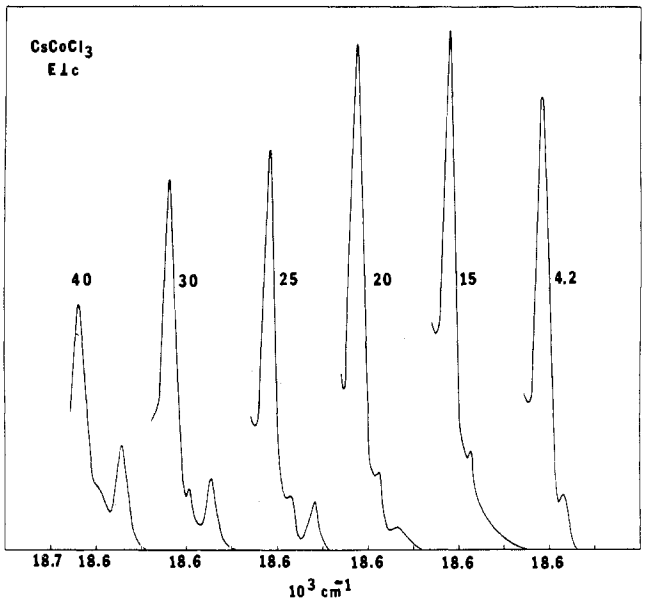

Figure 7. Sidebands associated with the $^2T_1(P)$ absorption in $CsCoCl_3$ with $E \perp c$ at several temperatures.

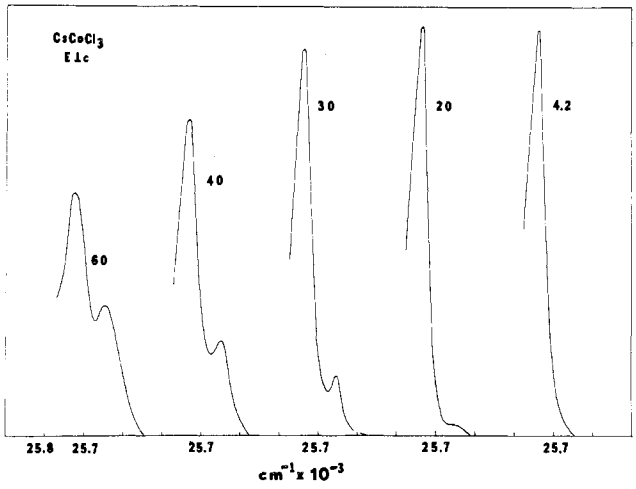

Figure 8. Sidebands associated with the $^2T_2(D)$ absorption in $CsCoCl_3$ with $E \perp c$ at several temperatures.

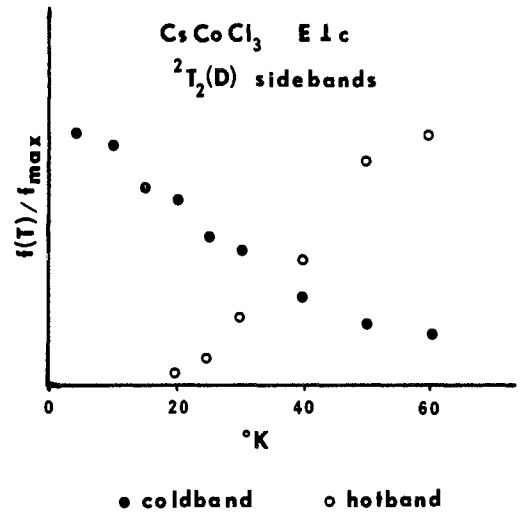

Figure 9. Temperature dependence of the oscillator strengths of the sidebands associated with the $^2T_2(D)$ absorption in $CsCoCl_3$ with $E \perp c$.

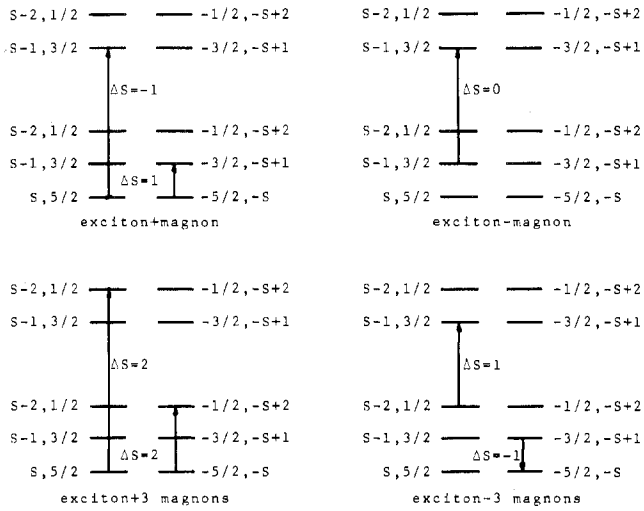

Figure 10. Schematic representation of exciton/magnon processes which lead to cold bands and hot bands. Positive and negative signs on the spin number, S, indicate the opposite sublattices of the antiferromagnet.

dependence is given in Figure 9. The cold band occurs at 25 733 cm^{-1} and persists through 80 K. The hot band appears above 15 K at 25 648 cm^{-1} and also persists through 80 K.

Discussion

The proposed mechanism of magnon sideband absorptions was developed for three-dimensional magnetic materials and involves two sublattices of the antiferromagnetic lattice.[29] The sublattices need be differentiated by spin alignment only, such that the total spin projections of the sublattices are equal in magnitude but opposite in sign. It is possible for a single photon to excite the sublattices individually or simultaneously. Thus if an excitonic transition is formally spin forbidden, the simultaneous excitation of the exciton on one sublattice and an appropriate magnon on the opposite sublattice conserves total spin since the magnon transition results in an equal and opposite change in spin. The spin excitations by magnon quanta are of sufficiently low energy that they may be of thermal origin. If this is the case, the apparent ground state of the sublattice is actually a magnon excited state which may then be of the same spin multiplicity as orbital excited states. Excitonic transitions between such states are then spin allowed. These processes and extensions of these concepts are represented in Figure 10. The absorptions involving thermally populated magnon ground states are termed magnon hot bands and occur at slightly lower energies than the pure exciton peaks. The absorption bands associated with transitions from the true ground state are favored by low temperature and are termed magnon cold bands. The cold bands occur to the high-energy side of the pure exciton peak.

As the titles imply the intensities of magnon hot bands and magnon cold bands vary with temperature in the opposite sense. Absorption processes resulting in cold bands have maximum probability at 0 K where thermal depopulation of the ground state ceases. As temperature is raised from this limit, transition probability decreases as thermal depopulation of the ground state increases. Near T_N the transition probability and resultant intensity decrease markedly as long-range order is lost. Hot-band processes, on the other hand, have zero probability at 0 K. As temperature is raised from 0 K, hot-band intensity becomes finite at some point and increases in proportion to the increasing occupancy of magnon states. Near T_N hot-band intensity should reach a maximum before long-range magnetic order is lost.

This mechanism has adequately explained the behavior of magnon cold bands observed in three-dimensional magnetic

materials;[5,15] however, when the measurements from the one-dimensional cobalt compounds are compared to the theory, several discrepancies are apparent. First, the hot bands appear just below T_N rather than increasing gradually in intensity from some point of appearance above 0 K. This behavior indicates that the three-dimensional exchange forces are sufficiently dominant at temperatures below T_N to hold the magnetic lattice fairly rigid with respect to thermal magnons. Only near the upper temperature limit of the three-dimensionally ordered phase does sufficient thermal magnon state population occur to allow observable hot-band processes. An additional contributing factor to this anomaly may be associated with the magnetic phase transition which occurs near 8 K within the ordered state.[25] The change in spin structure may include symmetry changes which alter selection rules so as to allow hot-band processes which were forbidden by symmetry in the low-temperature phase. The credibility of this argument must await the characterization of the spin structure near T_N.

The second deviation from theory apparent in our results is the lack of a pronounced correlation between T_N and the temperature region of largest change in sideband intensity. While it does appear that the intensity of the sidebands begins to change more rapidly near T_N, the change extends through a much broader range of temperature than is predicted. The sharp changes in intensity are predicted because of the loss of magnetic order above T_N. However, in the one-dimensional systems it appears that the transition from three-dimensional magnetic order to paramagnetism is not so abrupt as that in three-dimensional materials, that it extends over a relatively wide span of temperature, and that it may include a phase consisting of strong one-dimensional spin correlation. This phenomenon is also evident in the very broad maximum observed in magnetic susceptibility studies[30] and in inelastic neutron-scattering measurements which indicate one-dimensional spin waves above T_N.[31]

A third deviation from predicted behavior is manifested as a peaking or maximization of hot-band intensity well above T_N. The temperature of maximum hot-band intensity is the temperature at which optimum thermal population of magnon states occurs. Since this temperature is outside the range of three-dimensional magnetic order, the intensity is clearly a property of the one-dimensional system. The result can be seen to be compatible with the proposed mechanism and to provide further insight to the overall process of sideband absorption when the fundamental concepts of the mechanism are examined. While the mechanism, as summarized earlier, is based on magnetic sublattices of an antiferromagnet lattice, the arguments apply equally well to smaller aggregates of magnetic ions, even a pair.[11] In addition, there is no implicit requirement for permanent magnetic order. If an appropriately ordered array of spins existed on a time scale sufficient to allow an excitonic transition, the basic requirements of the mechanism would be satisfied. It thus appears that in the one-dimensional magnetic materials studied here, the intrachain exchange forces are of sufficient strength to maintain a degree of spin correlation sufficient to allow sideband absorption processes to temperatures far above T_N.

The final deviation from predicted behavior is the abrupt disappearance of the sidebands at $\sim 3T_N$. This is not a case of the peaks broadening beyond resolution or being masked by phonon broadening of the manifold; it is instead the disappearance of relatively sharp peaks in the span of a few degrees. The behavior can be understood when it is compared with magnetic susceptibility measurements. For $CsCoCl_3$ the temperature of sideband disappearance corresponds to the temperature at which the susceptibility first deviates from paramagnetic behavior.[30] The temperature at which sidebands disappear is then the temperature at which thermal quanta prevent even short-range, short-duration spin correlation and the material is totally in the paramagnetic phase.

Summary and Conclusions

The results of this investigation establish the existence of magnon sidebands in one-dimensional magnetic materials and thus provide not only a better characterization of this type of material but also a better characterization of the mechanism of sideband absorption. Considering these results in concert with magnetic and neutron diffraction studies it now appears that the transition from the paramagnetic phase to the three-dimensional antiferromagnetic phase proceeds through a phase of extended one-dimensional spin correlation which exists over a remarkably broad span of temperature. The process of magnon sideband absorption is operative in this temperature region of one-dimensional correlation as well as in the true ordered phase but is not operative in the paramagnetic phase. This also serves to confirm the role of magnetic interactions in these absorption processes.

This study has also revealed, in the surprising number of sidebands observed, that the materials $CsCoCl_3$ and $RbCoCl_3$ are by far the best source of information on magnon sidebands yet examined. Clearly, further experiments are called for to utilize the full potential of these materials in elucidating the microscopic processes operative in concentrated magnetic solids.

Acknowledgment. We thank B. B. Garrett for his interest and comments. This work was supported by NSF Grant GP 41056 and by the Office of Naval Research.

Registry No. $CsCoCl_3$, 15305-74-5; $RbCoCl_3$, 25719-27-1.

Supplementary Material Available: Two tables showing the energies of the observed maxima in the 4.2-K spectra of $RbCoCl_3$ and $CsCoCl_3$ and the octahedral, crystal field assignments and eight figures showing the temperature dependences of several of the side bands (13 pages). Ordering information is given on any current masthead page.

References and Notes

(1) Part 6: N. W. Alcock, C. F. Putnik, and S. L. Holt, *Inorg. Chem.*, **15**, 3175 (1976).
(2) To whom correspondence should be addressed.
(3) C. F. Putnik, G. M. Cole, B. B. Garrett, and S. L. Holt, *Inorg. Chem.*, **15**, 826 (1976), and references therein.
(4) Y. Tanabe and K.-I. Gondaira, *J. Phys. Soc. Jpn.*, **22**, 573 (1967).
(5) D. D. Sell, R. L. Green, and R. M. White, *Phys. Rev.*, **158**, 489 (1967).
(6) J. Ferguson, H. J. Guggenheim, and Y. Tanabe, *Phys. Rev.*, **161**, 207 (1967).
(7) L. L. Lohr and D. S. McClure, *J. Chem. Phys.*, **49**, 3516 (1968).
(8) J. Ferguson, H. J. Guggenheim, and Y. Tanabe, *J. Appl. Phys.*, **36**, 1046 (1965).
(9) J. Ferguson, H. J. Guggenheim, and Y. Tanabe, *Phys. Rev. Lett.*, **14**, 737 (1965).
(10) Y. Tanabe, T. Moriya, and S. Sugano, *Phys. Rev. Lett.*, **15**, 1023 (1965).
(11) J. Ferguson, H. J. Guggenheim, and Y. Tanabe, *J. Phys. Soc. Jpn.*, **21**, 692 (1966).
(12) J. Ferguson, H. J. Guggenheim, and Y. Tanabe, *J. Chem. Phys.*, **45**, 1134 (1966).
(13) K. Shinagawa and Y. Tanabe, *J. Phys. Soc. Jpn.*, **30**, 1280 (1971).
(14) T. Fujiwara and Y. Tanabe, *J. Phys. Soc. Jpn.*, **32**, 912 (1972).
(15) T. Fujiwara, W. Gebhart, K. Pentanides, and Y. Tanabe, *J. Phys. Soc. Jpn.*, **33**, 39 (1972).
(16) K. Ebara and Y. Tanabe, *J. Phys. Soc. Jpn.*, **36**, 93 (1974).
(17) H. Tanaha, *J. Phys. Soc. Jpn.*, **31**, 368 (1971).
(18) See J. F. Ackerman, G. M. Cole, and S. L. Holt, *Inorg. Chim. Acta*, **8**, 323 (1974), for a review of this class of compounds.
(19) J. F. Ackerman, E. M. Holt, and S. L. Holt, *J. Solid State Chem.*, **9**, 279 (1974).
(20) G. M. Cole, C. F. Putnik, and S. L. Holt, *Inorg. Chem.*, **14**, 2219 (1975).
(21) C. F. Putnik, G. M. Cole, and S. L. Holt, *Inorg. Chem.*, **15**, 2001 (1976).
(22) C. F. Putnik, G. M. Cole, and S. L. Holt, *Inorg. Chem.*, **15**, 2135 (1976).
(23) H. Soling, *Acta Chem. Scand.*, **22**, 2793 (1968).
(24) A. Enberg and H. Soling, *Acta Chem. Scand.*, **21**, 168 (1967).
(25) M. Melamud, H. Pinto, J. Makovsky, and H. Shaked, *Phys. Status Solidi B*, **63**, 699 (1974).
(26) V. J. Minkiewicz, D. E. Cox, and G. Shirane, *J. Phys. (Paris)*, **32**, C-892 (1971).
(27) W. B. Yelon, D. E. Cox, and M. Eibschütz, *Phys. Rev. B*, **12**, 5007 (1975).

(28) V. J. Minkiewicz, D. E. Cox, and G. Shirane, *Solid State Commun.*, **8**, 1001 (1970).
(29) We present here a very general and necessarily brief summary of the proposed mechanism. For detailed information the reader is referred to refs 4–17.
(30) N. Achiwa, *J. Phys. Soc. Jpn.*, **27**, 561 (1969).
(31) M. T. Hutchings, G. Shirane, R. J. Birgeneau, and S. L. Holt, *Phys. Rev. B*, **5**, 1999 (1972).

Contribution from the Wright and Rieman Chemistry Laboratories, Rutgers, The State University of New Jersey, New Brunswick, New Jersey 08903, and Bell Laboratories Murray Hill, New Jersey 07974

Resonance Raman Spectra and Electronic Structure of Binuclear μ-Oxo-Bridged Decahalo Transition Metal Complexes $M_2OX_{10}^{4-}$, M = Ru, Os, W

JOSEPH SAN FILIPPO, Jr.,*[1a] PAUL J. FAGAN,[1a] and FRANK J. DI SALVO[1b]

Received November 3, 1976 AIC60791N

Excitation profiles have been obtained for the structurally related, linear μ-oxo-bridged complexes $Ru_2OCl_{10}^{4-}$, $Ru_2OBr_{10}^{4-}$, $Os_2OCl_{10}^{4-}$, and $W_2OCl_{10}^{4-}$. They reveal that the intense, low-frequency, totally symmetric metal–oxygen–metal stretching vibration which is the dominant feature in the resonance Raman spectra of these ions is coupled to a single electronic transition involving electrons spanning the M–O–M group. These observations establish that the M–O–M unit in these complexes is an electronically unique, independent chromophore. The suggested assignment for this transition, based on the Dunitz–Orgel molecular orbital description of the π bonding in these complexes, involves the promotion of an electron from a nonbonding e_g orbital to an antibonding e_u orbital. The utility of these observations and conclusions as they relate to the electronic structure of other linear and near-linear μ-oxo-bridged complexes is discussed. In addition, a study of the magnetic susceptibility of $K_4W_2OCl_{10}$ suggests that the previous view of this material as consisting of a mixed valent ion W^{III}–O–W^{V} is incorrect, but is consistent with the view that the two tungsten centers share equivalent d^2 configurations and are antiferromagnetically coupled with an exchange energy of ~75 K. The nonzero susceptibility at low temperatures is most readily accounted for by this exchange, a significant spin–orbit coupling, and C_4 crystal field combining to produce Van Vleck coupling to an excited magnetic state.

Introduction

Early interest in linear μ-oxo-bridged transition metal complexes centered about their diamagnetism, the unusual (linear) geometry of the metal–oxygen–metal unit, and the significantly shorter than usual metal–oxygen bond distance. The initial novelty of these complexes has been gradually replaced by their near-routine acceptance as a common structural unit. The recent recognition that linear and near-linear μ-oxo-bridged transition metal complexes appear biochemically in such systems as the protein hemerythrin has provided added stimulus to the study of these complexes.[2]

We recently reported that Raman spectroscopy can provide a convenient spectroscopic technique for the detection and study of certain μ-oxo-bridged complexes.[3] In the specific examples examined viz., $M_2OX_{10}^{4-}$ (M = Ru, Os, W; X = Cl, Br), the Raman spectra were characterized by the intense, easily identifiable symmetric M–O–M stretching vibration, ν_1, with overtone progressions that extend in some instances to at least 6 ν_1 as well as a series of combination band progressions, the most outstanding of which corresponded to $n\nu_1 + \nu_2$ [$\nu_2 = \nu(M\text{–}X_{terminal})$] and $n\nu_1 + \nu_5$ [$\nu_5 = \nu(M\text{–}X_{radical})$]. As part of our continuing study of this class of compounds, we have examined this resonance effect in greater detail and report here the information it provides about the electronic nature of these complexes.

Experimental Section

Crystalline samples of $K_4Ru_2OCl_{10}$, $Cs_4Ru_2OBr_{10}$, and $(NH_4)_4[Os_2OCl_{10}]$ were prepared by previously described procedures.[3]

Raman spectra were determined on a Cary Model 82 spectrometer equipped with a triple monochromator and a krypton and an argon (Coherent Model 52) ion laser. Ultraviolet and visible spectra were determined on a Cary Model 14 spectrophotometer.

Solution Raman spectra were determined on freshly prepared, dilute samples in concentrations ranging from 2×10^{-4} to 5×10^{-3} M. The solubilities of several of the complexes was insufficient in the solvent of choice (5, 6, and 12 M HX) to permit the determination of their spectra. In these instances, the desired solubility was obtained by addition of 18-crown-6 ether. Spectra were determined using a rotating cell.[4a] Raman intensities were determined by adding a known amount of internal standard to the solution and comparing the intensity of the band of interest to that of the $\nu_1(A_1)$ line of the internal standard. At least three spectral scans were made for each determination and the peak areas were measured directly with a polar planimeter. The resulting intensity ratios were averaged, converted to a molar basis, and corrected for phototube response.

Solid-state Raman spectra were obtained with the aid of a rotating cell.[4b] Intensities were determined by adding a known amount of an internal standard such as KNO_3 to the desired μ-oxo-decahalo complex and homogenizing the mixture in a Spex Wig-L-Bug. Integration and normalization procedures were the same as those described for solution samples.

Tetrapotassium μ-oxo-decachloroditungsten(IV) was prepared by a modification of a procedure reported by Colton and Rose.[5] Tungstic acid, H_2WO_4 (12.5 g, 50.0 mmol), was added slowly with stirring to a warm (~75 °C) solution of potassium carbonate (7.5 g) in water (20 ml). The resulting slurry was filtered hot and the filtrate was diluted with water to a total volume of 30 ml. This solution was then added slowly with stirring to 300 ml of boiling concentrated hydrochloric acid. The resulting solution was cooled in an ice bath to ~18 °C and filtered, and the filtrate was treated (in ~1 g portions) with granular (325 mesh) tin (a total of ~8.5 g). Upon the sudden appearance of a deep violet color (~15–20 min from the time addition began), the solution was rapidly gravity filtered through a plug of glass wool into a cooled (0 °C) three-necked, 500-ml, round-bottom flask and the filtrate was saturated with HCl gas. After ~40 min, a crystalline material was observed and collected by suction filtration on a fritted glass funnel. The dark-green crystals, which occasionally appeared as an amorphous magenta powder when precipitated too rapidly, were washed with two 15-ml portions of cold (0 °C) absolute ethanol followed by three 10-ml portions of diethyl ether before drying in vacuo. The isolated yield was 2.2 g (10%). Anal. Calcd. for $K_4W_2OCl_{10}$: K, 17.48; Cl, 39.63; W, 41.10. Found: K, 16.91; Cl, 40.07; W, 39.84; Sn, <0.01.

Results

$Ru_2OX_{10}^{4-}$. The solution electronic spectra of the ions $Ru_2OCl_{10}^{4-}$ and $Ru_2OBr_{10}^{4-}$ are seen in Figures 1 and 2 and tabulated in Table I. They are, in general, poorly resolved, complex spectra. They reveal several parallel features that are noteworthy. Specifically, both spectra reveal a single, moderately intense band between 450 and 500 nm: $Ru_2OCl_{10}^{4-}$ (479 nm, ϵ 5200), $Ru_2OBr_{10}^{4-}$ (492 mn, ϵ 4900). Additional bands appear at higher energies in the spectra of both